Contents lists available at ScienceDirect

Additive Manufacturing

journal homepage: www.elsevier.com/locate/addma

Highlights

Fabrication and experimental characterisation of a bistable tensegrity-like unit for lattice metamaterials

Additive Manufacturing xxx (xxxx) xxx

Claudio Intrigila*, Andrea Micheletti, Nicola A. Nodargi, Edoardo Artioli, Paolo Bisegna

- Stereolithography fabrication of tensegrity-like units without pin-joints or cables.
- Experimental investigation on the compressive behaviour of a tensegrity-like unit.
- Bistable response of the designed unit confirmed by experimental results.
- Design procedure suitable to lightweight metamaterials with nonlinear behaviour.
- Tessellation of units for multistable metamaterials and control of compact waves.

Contents lists available at ScienceDirect

Additive Manufacturing

journal homepage: www.elsevier.com/locate/addma

Graphical Abstract

Fabrication and experimental characterisation of a bistable tensegrity-like unit for lattice metamaterials

Additive Manufacturing xxx (xxxx) xxx

Claudio Intrigila*, Andrea Micheletti, Nicola A. Nodargi, Edoardo Artioli, Paolo Bisegna

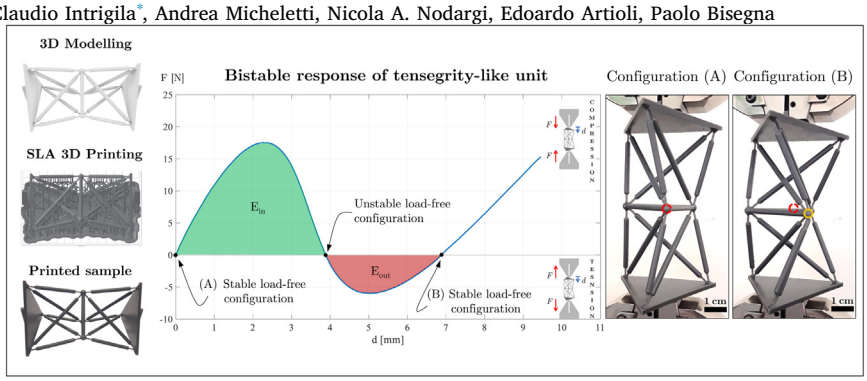

Contents lists available at ScienceDirect

Additive Manufacturing

journal homepage: www.elsevier.com/locate/addma

Research paper

Fabrication and experimental characterisation of a bistable tensegrity-like unit for lattice metamaterials

Claudio Intrigila *, Andrea Micheletti, Nicola A. Nodargi, Edoardo Artioli, Paolo Bisegna

Department of Civil Engineering and Computer Science, University of Rome Tor Vergata, Rome, Italy

ARTICLE INFO

Keywords:
Bistable systems
Additive manufacturing
3D printing
Tensegrity
Compression test

ABSTRACT

The peculiar nonlinear mechanical behaviour of tensegrity structures and their engineering applications have attracted considerable interest in the last two decades. However, the difficulties in their traditional fabrication and assembling methods represent current limitations to their widespread use. This paper presents a novel design and fabrication procedure for bistable tensegrity-like units. Starting from the classical triangular tensegrity prism and using stereolithography technology, a double tensegrity-like unit was designed and realised monolithically as a compliant mechanism. High repeatability of compression tests confirmed the activation of the designed bistable twisting mechanism in large displacements, proving that the bistability of a tensegrity-like unit with null selfstress and no cables can dependably be achieved. Numerical simulations showed that a reduced-order stick-and-spring model is able to provide predictions on the nonlinear mechanical behaviour of the unit in close agreement with experimental results. Low relative density and bistable characteristics make this type of tensegrity-like unit suitable to manufacture highly-customisable multistable metamaterials. The proposed procedure could be applied to transform and additively manufacture other types of tensegrity structures with different nonlinear responses into corresponding tensegrity-like versions.

1. Introduction

The past few years have seen a consolidation of the literature on mechanical metamaterials in conjunction with significant advancements in additive manufacturing (AM) techniques [1–3]. Much attention was given to periodic lattices with different repeating units realised by suitable AM methods [4–10]. Several studies showed that it is possible to attain unprecedented behaviours characterised for example by exceptional strength-to-weight ratio and stiffness-to-weight ratio [11–14], frequency bandgaps [15,16], negative overall elastic moduli or negative mass density [17–19], auxeticity [20], optimised piezoelectric properties [21,22], and solitary wave propagation [23,24].

A peculiar class of mechanical metamaterials is that of tensegrity metamaterials, that is, metamaterials whose units are designed as tensegrity structures [25,26]. Tensegrity structures are selfstressed pin-connected frameworks composed of struts and cables, which were shown to display a marked nonlinear response, dependent on the selfstress level, when subjected to static or dynamic loads [27,28]. In fact, in [29,30] it was demonstrated that, depending on their aspect ratio, tensegrity prisms exhibit a stiffening or softening response in compression tests. In addition, in [31] a particular tensegrity unit was found to possess two different bistable regimes, one triggered by changes in geometry, the other one triggered by an increase in the selfstress level. Such features can be effectively exploited for designing tensegrity metamaterials with a nonlinear response as periodic assemblies of tensegrity units. For example, in [23,24,32] one-dimensional arrays of tensegrity prisms were shown to support the propagation of solitary waves, and this result was generalised to two- and three-dimensional arrays of tensegrity units in [33].

One of the main challenges to overcome for the development of tensegrity metamaterials is their fabrication, given the difficulty of realising, assembling, and selfstressing cables. A handful of studies experimented with AM for the realisation of tensegrity structures. In [34], tensegrity structures were additively manufactured using rigid place-holder elements in the place of cables, which were replaced by elastic elements once AM was completed. In [35], self-deployable temperature-responsive tensegrity structures were manually assembled from additively manufactured bars and cables. In [36], arrays of tensegrity prisms were realised by AM of struts and bases of the tensegrity prisms, with the aid of temporary supports, followed by the installation and tensioning of cables. More recently, in [37], bars were 3D-printed in polylactic acid together with and inside a sacrificial water-soluble mould. The sacrificial mould also formed an internal channel network in which a liquid polymeric smart material was injected to realise

* Corresponding author.
E-mail address: intrigila@ing.uniroma2.it (C. Intrigila).

https://doi.org/10.1016/j.addma.2022.102946
Received 9 February 2022; Received in revised form 9 May 2022; Accepted 30 May 2022

cables. The latter were then cured by heating before the sacrificial mould was dissolved in water.

It is evident that the presence of selfstressed tension-only elements constitutes an obstacle for an effective AM of tensegrity metamaterials. However, this issue can be side-stepped by considering conventional lattices with tensegrity architecture, here referred to as *tensegrity-like structures*, which are able to mimic the nonlinear response of the corresponding tensegrity structures. This point was exemplified in [38], in which three-dimensional arrays of tensegrity-like units based on a bistable double triangular prism were designed, fabricated at the micrometre-scale by multiphoton lithography, and subsequently tested in compression. Test results showed a shift from a primary stable configuration to a secondary one. Still, it was not possible to shift the tensegrity-like structure back to the primary stable configuration since specimens could not be tested in tension at that scale. Furthermore, in [39], the impact response of a cuboctahedral tensegrity-like structure with elastically buckling struts was analysed, whereas, in [40], the tuning of the lowest frequency bandgap of a column-shaped modular tensegrity-like structure was performed. In both cases, tensegrity-like structures were realised in polyamide by selective laser sintering. In another study [41], compression tests were performed on periodic tensegrity-like structures realised by two-photon polymerisation direct laser writing, showing suppression of localised deformation and damage events and leading to a fully stable stress–strain response with an improved combination of failure resistance, energy absorption, deformability and strength with respect to conventional lattices. In all those studies, the observed behaviours can be ascribed to the tensegrity architecture of the lattices.

On starting from the unit presented in [38], the feasibility of fabrication of similar units at larger scales with more affordable AM methods, such as fused deposition modelling, was explored in [42]. Although the snapping response of the designed tensegrity-like unit was experimentally attained, the most attractive feature of bistability was not achieved. In fact, bistability is precisely at the base of multistable mechanical metamaterials with reversible and irreversible nonlinear behaviours that have been widely investigated for multifunctional engineering applications [43], including shape reconfigurable intelligent materials [37,44], reusable shock-impact resistance [45,46], energy trapping and absorption [45,47], sound and elastic wave propagation control [48].

This paper presents a novel design and fabrication procedure to achieve for the first time bistable tensegrity-like structures, which can then serve as repeating units in multistable lattice metamaterials. In particular, such procedure is demonstrated through the realisation of a double triangular prism structure as a compliant mechanism [49], with flexible hinges realised by reducing the cross section of lattice members over a short length near the nodes. Such bistable unit is specifically designed for performing tension–compression tests, and it is fabricated via inverted stereolithography technology. In order to investigate the mechanical behaviour and the main mechanical parameters involved in the response of the bistable tensegrity-like unit, specimens are tested under quasi-static compressive loading with displacement control. Finally, test results are used to validate the predictions of a reduced-order stick-and-spring model of the unit [50,51].

The high repeatability attained during the experimental campaign and the fairly good agreement with numerical simulations reveals that the bistable behaviour of additively manufactured tensegrity-like units with low relative density can be reliably achieved. Such results open a new scenario on the possibility of designing multistable tensegrity-like metamaterials, with freely tunable geometry and behaviour, for different multifunctional applications.

As the bistable unit considered in this work originates from the triangular tensegrity prism (Fig. 1 (a)), the present results could be extended to any prismatic tensegrity unit with N-sided polygonal base plates (Fig. 1 (b, c)). Additional extensions could be fulfilled using truncated polyhedral tensegrities [52,53] (Fig. 1 (d–f)) or multistage towers (Fig. 1 (g)). Indeed, the proposed procedure could be applied to transform any tensegrity system possessing one independent selfstress state and one independent internal mechanism into a bistable tensegrity-like unit. Other than the several known examples of tensegrity systems of this kind, new ones with desired features could be obtained by taking advantage of the many form-finding algorithms and analysis methods available in the literature (e.g., see [54–60]). In addition, the proposed design procedure could be used to realise units with nonlinear stiffening or softening behaviour as well. Finally, by guaranteeing the kinematic compatibility between internal mechanisms of adjacent units, these could tessellate the space via different assembly strategies to obtain lattice metamaterials with multistable or highly nonlinear behaviour. Fig. 1 (h–j) reports some literature examples of tensegrity and tensegrity-like tessellations.

The paper is organised as follows. The principal properties of tensegrity systems and tensegrity-like lattices are presented in Section 2.1, while the main parameters considered in the design are described in Section 2.2. The additive manufacturing process and the characterisation of the parent material are described in Section 3. Experimental results of the units tested under quasi-static compressive loading are reported in Section 4.1. In Section 4.2, numerical results obtained using a reduced-order stick-and-spring model are presented and compared with experimental ones. Finally, concluding remarks are outlined in Section 5.

2. Design of tensegrity-like lattices

2.1. From tensegrities to tensegrity-like structures

Tensegrity structures are free-standing pin-connected frameworks composed of bars, which can carry compression or tension, and cables, which can only carry tension. In stable configurations, such structures are subjected to a selfstress state in which member axial forces are in equilibrium with null loads. A tensegrity structure can possess first-order infinitesimal mechanisms, also called soft-modes. These are given by nodal displacements causing second-order member elongations [62], and they are associated with highly nonlinear behaviour and significant changes in configuration. For instance, it was shown in the literature that the simplest three-dimensional tensegrity structure, the triangular tensegrity prism, or T3 (Fig. 2 (a)), features a marked nonlinear response depending on its aspect ratio and level of selfstress, when subjected to loads activating its infinitesimal mechanism [27,29]. An analogy can be drawn between the T3 and the two-element system in Fig. 2 (b).

A T3 unit can be obtained by considering a triangular right prism or right frustum with cables placed along the edges, and non-contiguous bars placed along the diagonals of the lateral faces; in addition, one base is rotated with respect to the other one by a certain twist angle φ. Symmetric stable selfstressed configurations of a T3 are only required to have a twist equal to $\pi/6$ (Fig. 2 (a)), while the height of the prism/frustum and the size of each triangular base can be chosen arbitrarily.

T3 units possess one independent infinitesimal mechanism and one independent selfstress state. In the mechanism, there is a relative motion between the top and bottom bases given by a vertical translation accompanied by a rotation about the vertical axis. The blue arrows in Fig. 2 (a) represent the possible nodal displacement vectors in such a motion, assuming the bottom base fixed. Fig. 2 (a) also shows the selfstressing axial forces applied to one of the nodes. A corresponding illustration is given in Fig. 2 (b) for the analogous two-element system. The representative force-vs-displacement curve for a vertical downward load applied to the T3 unit and to the two-element system in Fig. 2 (a, b) is shown in Fig. 2 (c), solid line, considering linearly elastic bars and cables and a large-displacement regime. The slope at the origin, $\tan\alpha$, is directly proportional to the level of selfstress [63], and vanishes for a null prestress (dashed curve in Fig. 2 (c)).

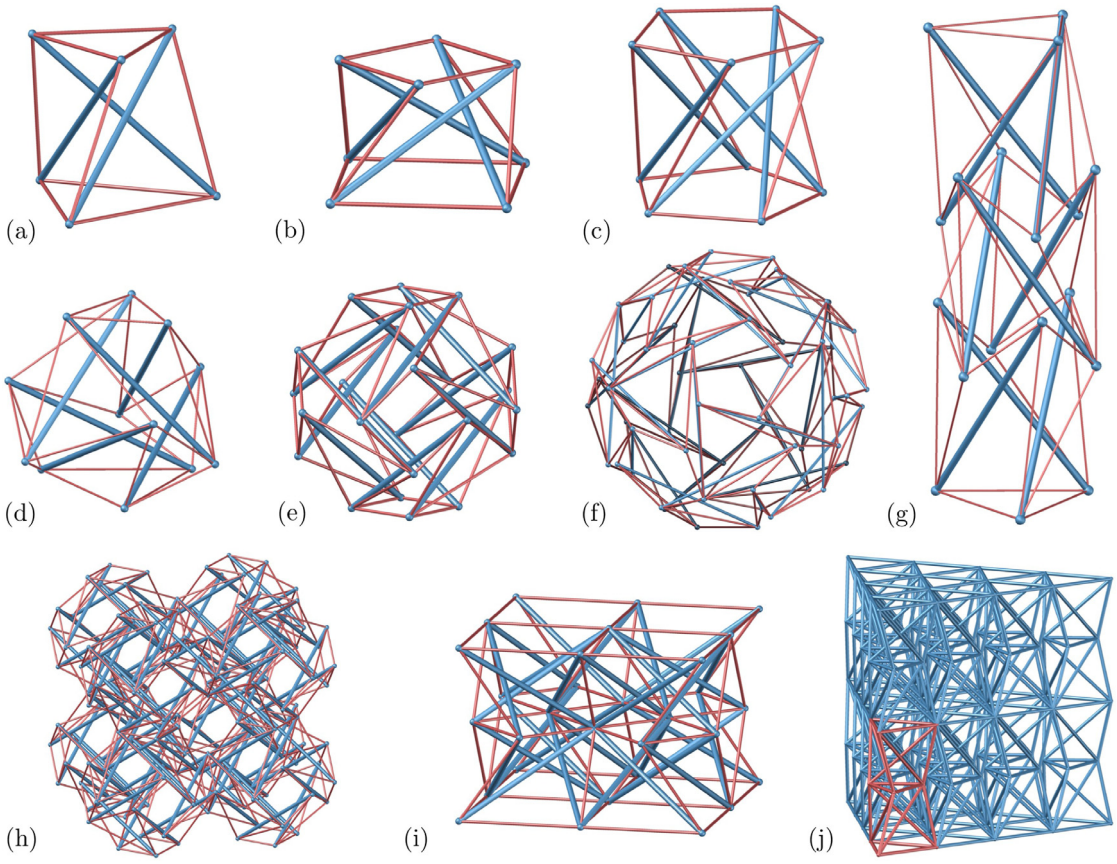

Figure 1. Examples of tensegrity units and some possible spatial tessellations. (a–c) Triangular, square, and pentagonal tensegrity prisms. (d–f) Diamond tensegrity units: truncated tetrahedron, octahedron, and icosahedron. (g) A three-stage tensegrity tower with triangular base. (h) An assembly of truncated octahedral units, similar to those proposed in [53]. (i) An assembly of square tensegrity prisms, similar to those in [61]. (j) A tensegrity-like lattice based on a double triangular prism, redrawn from [38]. See also [60] for a general method of unit generation.

The transformation from a tensegrity unit to a tensegrity-like one can be performed starting from a stable selfstressed configuration (*step i*). In order to achieve a bistable response, the selfstress sign is reversed, provided all cables are replaced with bars (*step ii*). Such bar framework is depicted in Fig. 2(d), and the analogous two-element system is shown in Fig. 2(e). This bar framework is characterised by a force–displacement curve featuring a negative slope at the origin (solid line in Fig. 2(f)), thus implying the existence of three load-free equilibrium configurations. In fact, the initial selfstressed configuration has become unstable, whereas the other two are stable, stress-free, and displaced in opposite directions along the mechanism [63]. One of the latter two configurations is chosen as the new reference configuration (*step iii*). In particular, for a bar framework based on a symmetric T3, that amounts to changing the value of the twist, that is, by setting $\varphi = \pi/6 - \theta_0$, with θ_0 the relative twist. Such bar framework is shown in Fig. 2(g), while the analogous two-element system is shown in Fig. 2(h). Fig. 2(j) shows the representative load-vs-displacement curve of systems (g, h), typical of a bistable response, subject to vertical loads. It can be observed that the larger the value of the relative twist θ_0, i.e., the higher the selfstress in the unstable configuration, the more marked the peaks.

A tensegrity-like unit is obtained from such a bistable bar framework by considering the corresponding monolithic spatial frame, i.e., characterised by the same nodal positions and connectivity, but composed of beam elements fully connected to nodes (*step iv*). As a consequence of replacing pin connections with built-in ones, the tensegrity-like unit is subjected to axial and shear forces, bending and torsion, and, in general, it may be no longer characterised by a bistable response. In order to recover such a peculiar behaviour, compliant hinges are introduced at nodes by a suitable reduction in the cross section of the beams near the nodes (*step v*).

The static behaviour of the obtained tensegrity-like unit is exemplified in Fig. 3 by resorting to a stick-and-spring model [50,51]. Bars are extensible but otherwise rigid, and compliant hinges are modelled as rotational springs responding to the change in angle between adjacent bars. Fig. 3(a, b) shows the T3 tensegrity-like unit with rotational springs (symmetric copies not shown) and the analogous two-element system, respectively. Fig. 3(c) shows the response of the unit for increasing values of the rotational spring constant k_r. It can be observed that for small values of k_r there are still two stable load-free equilibrium configurations, while for large values of k_r the system is not bistable, but it still has a snapping response. Fig. 3(d) shows the elastic energy of a tensegrity-like structure, E, as the sum of the energy of the bar framework, E_b, plus the rotational spring energy, E_r. Hence, to preserve the bistable feature, a suitable choice of link geometry is crucial to keep the force–displacement curve close enough to that of the corresponding pin-connected structure.

Finally, the obtained monolithic structure can be fabricated by AM techniques (*step vi*). Regarding the experimental characterisation, the elasticity of the testing machine or connectors may be taken into account in the measured response. This effect can be modelled by an additional axial spring with constant k_p connected in series to the two-element system shown in Fig. 3(e, f). For a given value of the load F, the force-vs-displacement curve is modified by the additional displacement $d_p = F/k_p$ (Fig. 3(f)).

2.2. The double-T3 unit

The double-T3 unit proposed in [38] is here chosen to perform a compression–tension experiment. It was obtained by reflection and

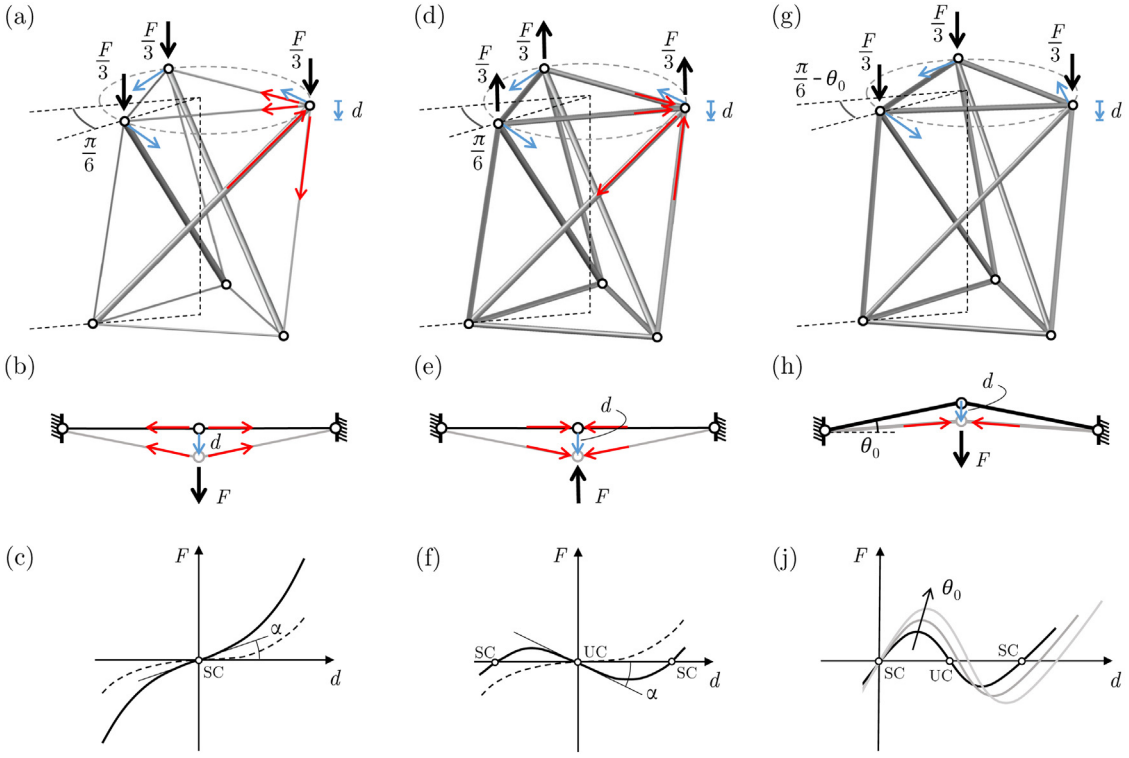

Figure 2. (a) A prismatic T3 unit. Top and bottom bases are rotated with respect to each other by a twist angle of $\pi/6$. The blue arrows represent the nodal displacement vectors at each node in the mechanism assuming the bottom base fixed. The red arrows represent the selfstressing forces at a node. (b) Two-element structure in two dimensions analogous to the T3. (c) The characteristic nonlinear stiffening response to vertical loads for systems in (a) and (b) with initial stable configuration (SC). The slope at the origin increases with prestress level. (d, e) Bistable bar framework corresponding to systems (a, b) obtained by reversing the selfstress sign and replacing cables with bars. (f) Representative bistable response of systems (d) and (e) for vertical loads, featured by three load-free equilibrium configurations. The initial one is unstable (UC) and the other two stable (SC). (g, h) Bistable bar framework corresponding to systems (d, e) obtained by choosing one of the SCs as reference configuration, i.e., by introducing a slight change in geometry with respect to the UC, measured by the parameter θ_0. (j) Representative bistable response of systems (g) and (h) for vertical loads and the influence of θ_0 on the structural behaviour.

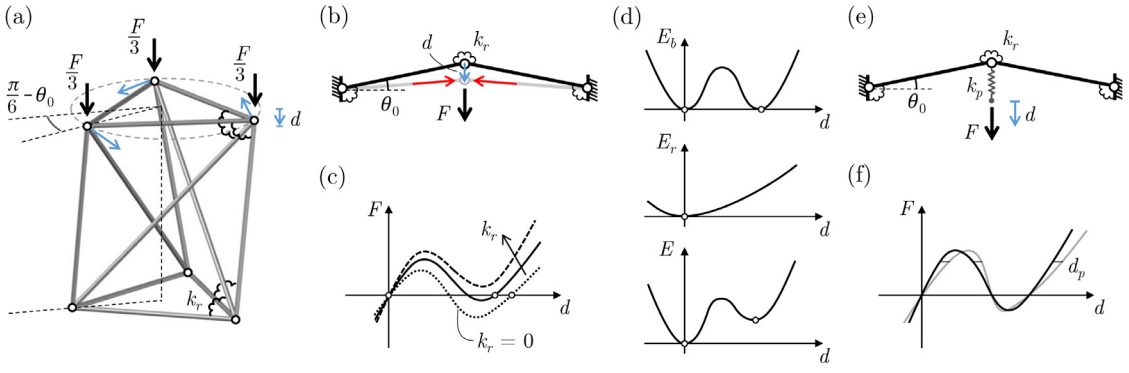

Figure 3. (a) The T3 tensegrity-like unit with rotational springs (symmetric copies not shown). (b) The analogous two-element system. (c) Force-vs-displacement curve for increasing values of the rotational spring constant k_r. Stable load-free equilibrium configurations are marked by white dots. (d) The elastic energy of a tensegrity-like structure, E, is given by the energy of the bar framework, E_b, plus the rotational spring energy, E_r. (e, f) Effect of an additional axial spring with constant k_p connected in series to the two-element system. For a given value of the load F, the force-vs-displacement curve is modified by the additional displacement $d_p = F/k_p$.

juxtaposition of two equal frustum T3 tensegrity-like units with a chosen relative twist. In Fig. 4, the top T3 is the mirror image of the bottom T3 with respect to the plane containing the middle base. In this way, the relative rotations in each T3 mechanism are opposite to each other, allowing for a purely translational relative motion between the upper and lower bases. The cyclic-symmetric wireframe geometry of such an assembly is determined by: the relative twist, θ_0, the same for both T3s; the height of the T3, h; the circumscribed radius of the outer bases, a; and the circumscribed radius of the middle base, b (Fig. 4 (a)).

The parametric geometry of the tensegrity-like unit was developed via the Grasshopper object programming language, available as a plug-in of the CAD Rhinoceros 3D software. Starting from the wire-frame model of the double-T3 shown in Fig. 4 (a), the nodes were realised as spheres of diameter d_s, while the beams forming the middle base were realised with a solid circular cross section of diameter d_b. The beams placed between the outer and middle bases were subdivided into three segments: the bar main body, with constant cross section d_b, and two end links of length l_l to form the connections with nodal spheres. In particular, each link was designed using a spline profile: its central part has a solid circular cross section of almost constant diameter d_l and net length $l_n = l_l/2$, while at its ends there are smooth transitions between the larger diameters of the spheres and bar main body (Fig. 4 (c)).

Since the applied load can be compressive (positive) or tensile (negative) during the test, the outer bases are specially designed to fit

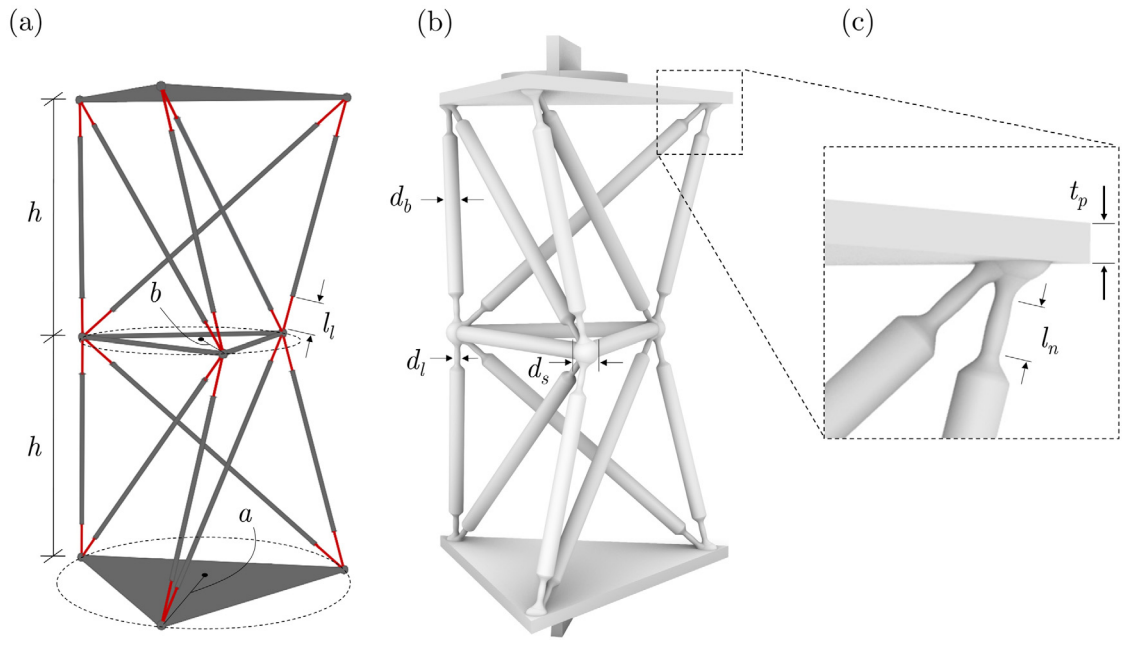

Figure 4. Geometry of the designed tensegrity-like lattice: (a) main geometrical parameters of the wire-frame model; (b) final 3D geometry; (c) detail of the nodal area between links and plate.

the grips of the testing machine. Each base is conceived as a triangular plate of thickness t_p with the addition of two orthogonal plates with the same thickness to ensure the clamping of the grips and a uniform load transfer to the tensegrity-like unit (Fig. 4 (b)).

Parametric simulations and preliminary testing of fabricated samples were performed to analyse the influence of the main design parameters on the mechanical response of the double-T3 unit and its bistable characteristics. Simulations, carried out by using a stick-and-spring model [50,51], are discussed in Section 4.2 (see also Figures S4–S9 of the SI). Parameters a, b, and h were set equal to 40 mm, 30 mm, and 60 mm, respectively, by considering the clearance between adjacent beams and the printing volume of the 3D printer. The values of relative twist, θ_0, link diameter, d_l, link length, l_l, net link length, l_n, and thickness of the triangular plate, t_p, were chosen reasoning as follows. It is observed that the larger θ_0, the larger the peak forces, potentially counteracting the adverse effect that the stiffness of compliant hinges, k_r, may have on bistability. Conversely, the smaller d_l, the smaller k_r and the link strain. However, d_l is bounded from below by the resolution of the 3D printer. A reduction of l_l produces a mechanism closer to that of the corresponding pin-connected framework; however, it makes k_r larger and increases the link strain. In order to obtain a bistable compliant mechanism able to undergo large nodal displacements without yielding, the final choice was: $\theta_0 = 11°$, $d_l = 1.6$ mm, $l_l = 10$ mm, $l_n = 5$ mm, and $t_p = 3$ mm, respectively. It is worth noticing that the geometry specified above corresponds to a volume fraction of the solid material, or relative density, $\bar{\rho} = 4.14\%$, a value which compares well with those recommended in the relevant literature [39,41].

3. Materials and methods

Over the last decade, the prompt advances in the AM sector have allowed addressing new challenges related to the manufacturing of complex mechanical metamaterials at different scales via different AM techniques, including direct laser writing [5], two-photon lithography [64], multiphoton lithography [38] and direct ink writing [65]. In the present work, the tensegrity-like lattice samples were fabricated using the inverted stereolithography (SLA) technology. In particular, the samples were fabricated with the desktop 3D printer Form 3B from Formlabs®. This printer exploits the low-force stereolithography technology, drastically reducing the forces exerted on parts during the print process and ensuring high prototyping accuracy. The resin used for printing was Tough 2000, produced by Formlabs. Although the composition of the material is not disclosed by the manufacturer, the Tough 2000 resin guarantees larger elastic deformation than traditional resins, maintaining a strength similar to polymeric materials such as acrylonitrile butadiene styrene or polylactic acid. The additive manufacturing process and the sample testing method are described in Section 3.1, whereas the characterisation of the parent material is presented in Section 3.2.

3.1. Sample fabrication and testing

The workflow of the main fabrication steps is summarised in Fig. 5. Starting from the CAD model transformed into an STL file, the geometry of the specimen is divided into sequentially thin layers bonded together, employing the PreForm slicing software. With this technology, the resolution of the layers is controlled by a modulation of the optical dimension of a high-power ultra-violet (UV) laser. Such resolution varies from 25 to 300 μm, also depending on the resin used. The samples were printed setting a 50 μm thickness layer and 25 μm XY plane resolution. In addition, given the complexity of the structural geometry, the samples were arranged horizontally, and suitable supports were designed, ensuring the hold of the sample and preventing any shifting during the printing process (see also Fig. 5 (b)).

After the 3D printing, two finishing steps are required to achieve the highest mechanical properties of the material and the best quality of the print: washing and post-curing. The former step allows removing the uncured resin from the surface of the printed parts by immersing and shaking them in a cleaning chamber filled with solvent. The latter step consists of a second polymerisation process in an oven, forming new polymer chains cross-linking via simultaneous exposition to UV light and high temperature. The two finishing steps were performed using Form Wash and Form Cure devices by Formlabs, respectively. Following the guideline specifications of the producer, the samples were washed in the Form Wash filled with tripropylene glycol monomethyl ether (TPM) for 10 min and then soaked in a fresh TPM basket for further 10 min. Once the washing process was completed, the samples

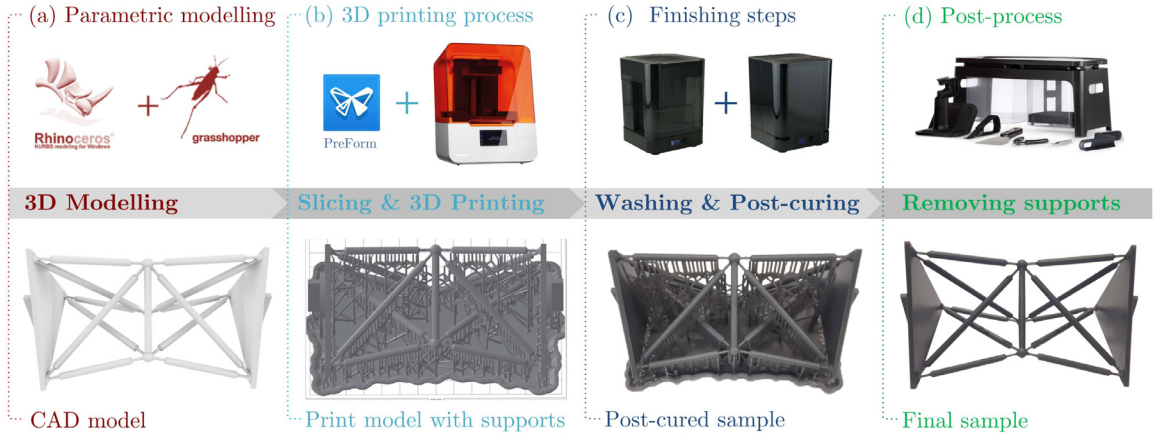

Figure 5. Workflow of the fabrication process: (a) parametric modelling and CAD model generation; (b) slicing and additive manufacturing via UV laser; (c) washing in a solvent bath and post-curing; (d) removing supports.

were dried using a compressed air machine. In order to achieve the highest mechanical properties of the Tough 2000 resin, the curing time and temperature were set at 120 min and 80°C, respectively. In fact, as pointed out in [66], a long post-curing at high temperature produces an increase of stiffness and strength of the Tough 2000 resin, maintaining a ductile behaviour. Fig. 5 (c) shows the sample after the post-curing process. Finally, the supports were removed (Fig. 5 (d)). Then, the samples were weighed, and the main geometric dimensions were checked with a calliper with a resolution of 10 μm.

The compression tests were conducted under quasi-static displacement-control, employing an INSTRON 4482 universal testing system equipped with a 10 kN load cell. The displacement rate used in the tests was 1 mm/min. Data were collected with an acquisition frequency of 20 Hz, while the tests were recorded with a camera sampling rate of 60 fps at 1080 p resolution. Three specimens were fabricated, and five repeat tests were performed for each printed specimen for statistical and repeatability purposes. The time interval between test repetitions was set equal to three hours in order to limit viscous and ageing effects.

3.2. Parent material

With the aim to evaluate the mechanical characteristics of the parent material, five type IV tensile specimens were manufactured, as prescribed in the ASTM D638-14 [67]. Following those standards, tensile tests were performed on the specimens using the INSTRON 4482 universal testing machine. A 10 kN load cell was used to record the forces. The tests were carried out under displacement control with a constant speed of the mobile crosshead set at 5 mm/min. An extensometer was applied to the specimen, ensuring accurate measurement of the gauge-length deformations. The signals of the instruments were acquired at a sampling rate of 20 Hz, and the tests were recorded with a digital camera, with a sampling rate of 30 fps.

The resulting nominal stress–strain curves of the five specimens under uniaxial tensile loading are plotted in Fig. 6. The trend of the curves exhibits an essentially ductile behaviour of the parent material, similar to the one shown in [66]. The mechanical properties derived from the tensile tests are summarised in Table 1, showing high repeatability of the measurements.

4. Results and discussion

4.1. Compression experiments

With the aim of developing tensegrity-like units with a tunable bistable behaviour, the experimental study focused on the compressive response of SLA-made double-T3 lattices. Moreover, attention

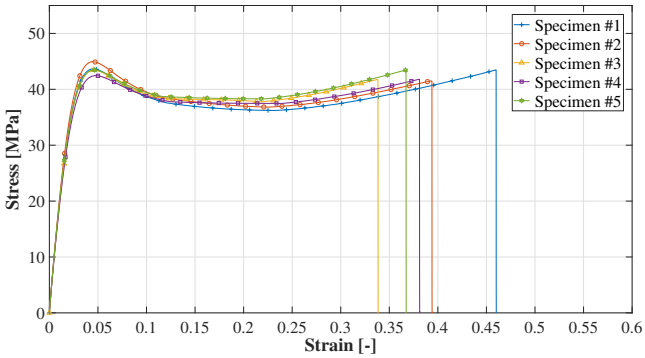

Figure 6. Tensile stress–strain curves of the resin Tough 2000. The test speed was set at 5 mm/min, according to ASTM D638-14 [67].

Table 1
Results of the tensile tests. The test speed was set at 5 mm/min, according to ASTM D638-14 [67].

Specimen #	Tensile peak [MPa]	Strain at peak [%]	Young's modulus [MPa]
1	43.7	4.65	2109
2	44.9	4.40	2125
3	43.4	4.47	2050
4	42.4	4.62	2021
5	43.5	4.68	2091
Mean±std	43.6±0.9	4.56±0.12	2079±43

was addressed to the main mechanical parameters deduced from the force–displacement curves such as limit loads, stiffness and trapping energy [45].

Fig. 7 (a) depicts the typical capacity curve of the proposed tensegrity-like unit under uniaxial compression load and the geometric representation of the main mechanical parameters investigated. As a general observation, the response of the double-T3 unit is characterised by a highly non-linear behaviour, accompanied by a significant geometric transformation between the undeformed and deformed configurations, as shown in Fig. 7 (b). The capacity curve can be divided into three segments: (i) the first stable branch up to the positive limit load, (ii) the unstable branch between the two limit loads, and then (iii) the second stable branch, crossing through the second stable load-free equilibrium configuration.

Moving from the initial configuration, even at small displacements (stage (A)), a non-linear relationship between force and displacement is

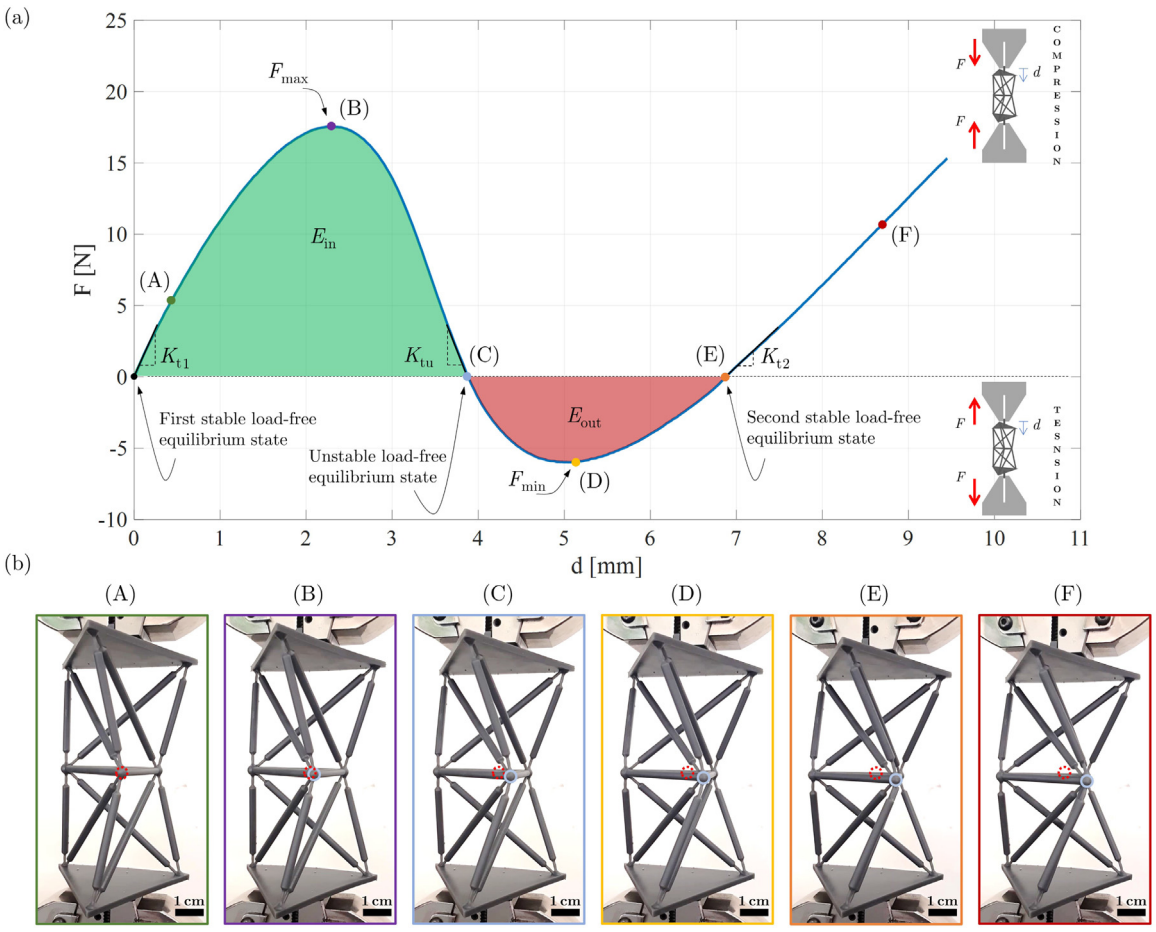

Figure 7. Compression testing results on double-T3 tensegrity-like unit: (a) force-vs-displacement curve and main mechanical parameters analysed; (b) selected deformed stages denoted by (A)-(F) in the force-vs-displacement curve. The red circular marker is kept fixed, whereas the white one follows the unit deformation.

observed. At an imposed vertical translation of about 2.2 mm, the compressive limit load (F_{max}) is reached, which represents the transition from the stable branch to the unstable one. In this configuration, it is possible to appreciate the anticlockwise rotation about the vertical axis of the middle triangle with consequent increase of the twist (φ), as depicted in the deformation stage (B). As the displacement increases, the force decreases until the unstable load-free equilibrium configuration is reached (stage (C)). At this stage, the theoretical twist value of the corresponding pin-connected framework is equal to $\pi/6$. However, the presence of compliant hinges characterised by a finite value of stiffness (k_r) implies a value of φ slightly greater than $\pi/6$, as shown in Fig. 3 (c).

The slope of the unstable branch (K_{tu}) is higher than the one obtained for the first stable branch (K_{t1}). As observed in Fig. 3 (e, f), the introduction of the two plates determines an additional displacement d_p under the force F, with a consequent reduction in the slope of the first stable branch and an increase, in absolute value, of that relative to the unstable branch.

After the unstable load-free equilibrium configuration, the sign of the load changes, and the force-vs-displacement diagram presents a region with tensile force (negative). The unstable branch terminates with the negative limit load (F_{min}), corresponding to the deformation stage (D), leading the system into the second stable branch. Then, as the imposed displacement increases, the equilibrium path approaches the second stable load-free equilibrium configuration (stage (E)). At this stage, the response of the system is deeply influenced by geometric nonlinearities. The change in angle between the adjacent bars produces significant deformation of the compliant hinges, required to accommodate the considerable twisting of the middle triangle.

Once the second stable load-free equilibrium configuration is overcome, the load becomes compressive again, and the equilibrium path shows an almost linear trend. The test was stopped at a load value close to the compressive limit load. From a kinematic point of view, the theoretical limit displacement of the bistable mechanism would be reached at $\varphi = \pi/3$, leading to contact between diagonal bars. It is worth noting that, by snapping between two stable load-free equilibrium configurations, the double-T3 unit is able to trap part of the energy introduced into the system during the loading process. In particular, this energy trapping is ascribable to the rotational energy stored by the links, E_r, as shown in Fig. 3 (d).

Five repetitions of the compression test were performed for each sample, assuming a time interval between each repetition equal to three hours in order to limit viscous and ageing effects. The force–displacement curves relative to the first printed samples are shown in Fig. 8, whereas the results of all tests on the three samples are reported in Figure S2 of the Supplementary Information (SI). The compressive response of the samples reveals high repeatability. The bistability was achieved in all tests with a trend that essentially retraces the one described in Fig. 7. The corresponding mechanical parameters deduced from the response curves of the three samples are reported in Table 2. The limit loads were evaluated as the positive (compressive) peak of the first stable branch (F_{max}) and the negative (tensile) peak of the unstable branch (F_{min}). Three tangent stiffnesses were considered as the slopes at load-free equilibrium configurations of the first and second stable branches (K_{t1} and K_{t2}, respectively), and of the unstable branch (K_{tu}). The trapped energy is equal to the area subtended by the force–displacement curve, evaluated as the difference between E_{in} and E_{out}, as shown in Fig. 7 (a).

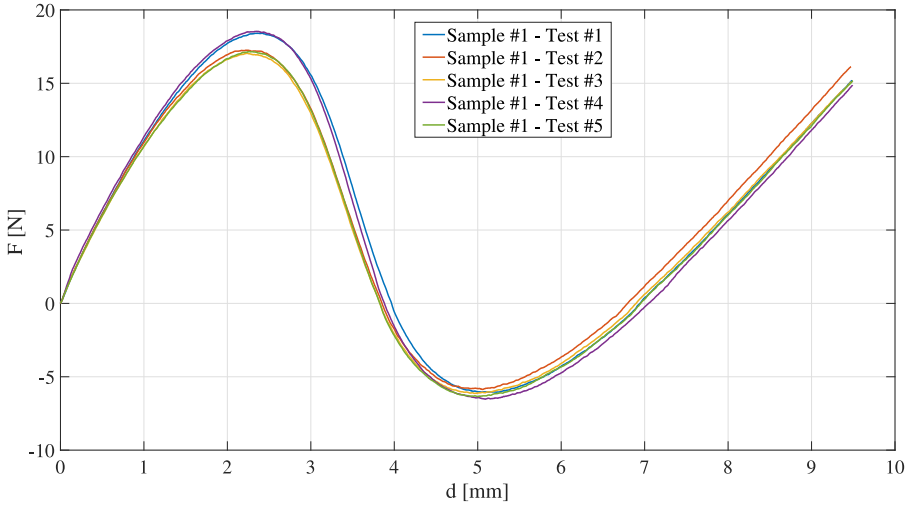

Figure 8. Uniaxial compressive response of tensegrity-like lattices: force–displacement curves of five tests on the first printed sample. The test speed was set at 1 mm/min. The curves relative to the second and third samples are reported in Figure S2 of the SI.

Table 2
Mechanical parameters deduced from the response curves of the three samples (see also Figure S2 and Table S1 of the SI) in terms of limit loads (F_{max}, F_{min}), tangent stiffnesses (K_{t1}, K_{tu}, and K_{t2}), and energy exchanged with the system during loading (E_{in}, E_{out}).

Tensegrity #	K_{t1} [N/mm]	K_{tu} [N/mm]	K_{t2} [N/mm]	F_{max} [N]	F_{min} [N]	E_{in} [mJ]	E_{out} [mJ]
1	11.7±0.2	−16.7±0.7	5.7±0.2	17.7±0.7	−6.2±0.3	43.6±2.5	−12.5±0.9
2	12.1±0.2	−16.7±1.3	5.8±0.0	18.8±0.7	−5.8±0.2	46.6±2.1	−11.3±0.6
3	11.4±0.1	−14.2±1.2	5.4±0.2	16.5±0.8	−5.1±0.6	40.0±2.6	−9.5±1.8
Mean±std	11.8±0.3	−15.8±1.6	5.7±0.2	17.6±1.2	−5.7±0.6	43.4±3.5	−11.1±1.7

Small values of standard deviation were obtained for the parameters analysed, confirming good repeatability of the tests. Slightly higher differences can be observed in the test repetitions relating to the third sample (see also Figure S2 (c)), possibly due to small variations of unaccounted variables, such as humidity and temperature levels during the test, or slight imperfections in the printing process. The significant difference between the values of E_{in} and E_{out} shows the capability of the unit to lock energy during the loading process, paving the way for designing double T3 unit layers to harness multiple absorption mechanisms. Further mechanical parameters characterising the force-vs-displacement curve are reported in Table S1 of the SI. In addition, the movie of the first test of each sample is included as Movie S1, S2 and S3 in the SI, respectively.

4.2. Numerical simulations

Numerical simulations were performed by resorting to a stick-and-spring model [50], which was already employed in [51] to simulate selfstressed tensegrity-like structures in dynamics. That is a reduced-order model accounting for geometric nonlinearities in a large-displacement regime. The unit is modelled as a pin-connected bar framework equipped with rotational springs. Bars can only lengthen or shorten while remaining straight, i.e., they behave as axial springs. Rotational springs are associated to certain pairs of adjacent bars, and they respond to the change in angle between them. The elastic energy of such a structure, assuming a linearly elastic constitutive behaviour of axial and rotational springs, can be written as:

$$E(\mathbf{p}) = \frac{1}{2}\left(\sum_i k_{ai}(\ell_i(\mathbf{p}) - \bar{\ell}_i)^2 + \sum_j k_{rj}(\psi_j(\mathbf{p}) - \bar{\psi}_j)^2\right), \tag{1}$$

where the vector $\mathbf{p}$ contains the nodal coordinates; ℓ_i, $\bar{\ell}_i$, and k_{ai} are respectively the current length, fabrication length, and spring constant of the ith axial spring; ψ_j, $\bar{\psi}_j$, and k_{rj} are respectively the current angle, fabrication angle, and spring constant of the jth rotational spring. Internal forces and couples are given by $t_{ai} = k_{ai}(\ell_i(\mathbf{p}) - \bar{\ell}_i)$ and $t_{rj} = k_{rj}(\psi_j(\mathbf{p}) - \bar{\psi}_j)$ for the ith axial spring and the jth rotational spring, respectively.

For the double-T3 tensegrity-like unit object of this study, the location of the rotational springs in each of the two T3s is shown in Fig. 3 (a) (symmetric copies not shown). Relevant quantities in Eq. (1) are computed by considering the geometry of the unit (Section 2.2), and by taking the Young's modulus $Y = 2079$ MPa (Section 3.2). Details of such calculations are given in the SI.

Tension–compression testing was simulated in a regime of large displacements and rotations by computing the tangent stiffness operator as the Hessian of the elastic energy [50], and by adopting a conventional Newton–Raphson numerical resolution procedure. Supports at the bottom are considered fixed in space, while the top supports are assigned a step-by-step increasing downward displacement. At each step, the applied load is computed as the resultant of the balancing support reaction forces.

Fig. 9 shows the force-vs-displacement curve obtained from the numerical simulation, which agrees fairly well with the curve computed as the average of all the tests on the three samples. Numerical simulations capture the initial stiffness and limit loads satisfactorily, both in compression and tension. A slight deviation of the force-vs-displacement curve can be observed at the unstable and second stable branches. This deviation could be explained by noting that the centres of relative rotation between bars are located at the nodes in the stick-and-spring model, while that is not generally the case in the fabricated tensegrity-like unit.

In the design of the double-T3 unit, the effect of geometric parameters on the mechanical response and its bistable characteristics was identified through parametric simulations whose results are reported in Figures S4–S9 of the SI. Specifically, results show that the relative twist angle is the most significant parameter and measures how far the configuration of the tensegrity-like structure is from the original tensegrity configuration. The relative twist angle affects both limit loads, in

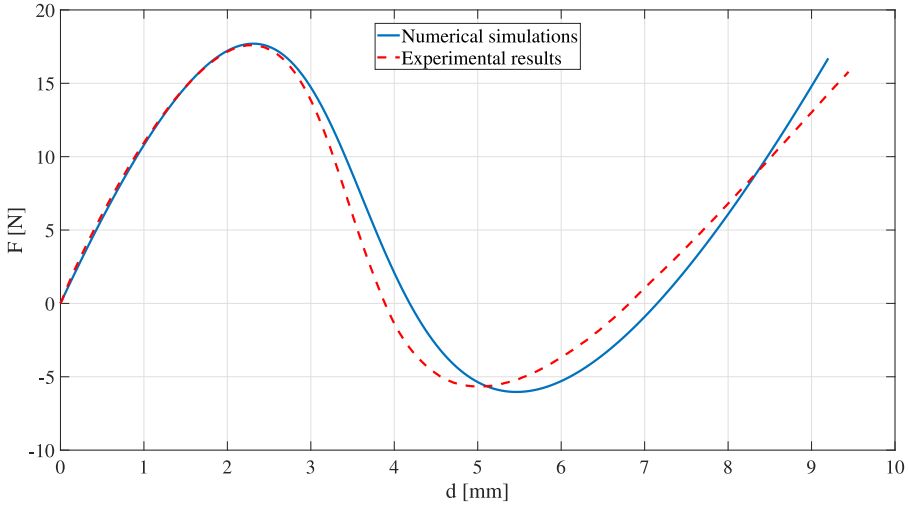

Figure 9. Comparison of force-vs-displacement curves obtained by numerical simulations (solid blue line) and experimental results (average of all tests on the three samples, dashed red line).

compression and in tension, as well as displacement values at load-free equilibrium configurations (cf. Fig. 2(j) and Figure S4 of the SI). The bending stiffness of the terminal links is directly related to the energy gap between the two stable load-free equilibrium configurations. On the one hand, the limit case of a pin-connected bistable structure is obtained considering a null value of the bending stiffness of the links, and it corresponds to no energy trapping (cf. Figure S5 of the SI). On the other hand, by increasing such stiffness, the unit can entrap more energy; however, if this stiffness is too large, the unit would lose the bistable feature (cf. Fig. 3(c)). In order to limit the bending stiffness of the links, it may be preferable to decrease their cross-sectional diameter rather than to increase their length (cf. Figures S6 and S7 of the SI) since the latter should stay as short as possible to maintain the kinematics close to that of the original tensegrity system. Finally, as the b/a ratio increases, the limit forces and displacement values at load-free equilibrium configurations rise rapidly, while the opposite effect is found as the h/a ratio increases (cf. Figures S8 and S9 of the SI).

5. Concluding remarks

The main goal of this work was to establish a novel design and fabrication procedure for a bistable tensegrity-like repeating unit for lattice metamaterials. Such procedure, which could be extended to other types of units, is summarised as follows: (i) start with a stable tensegrity system having one selfstress state and one internal mechanism; (ii) replace cables with bars; (iii) slightly modify the configuration by displacing nodes along the mechanism; (iv) replace pin connections with built-in ones and generate the solid geometry of the tensegrity-like structure with solid spheres at the nodes; (v) introduce compliant hinges by equipping bars with terminal links; (vi) fabricate the tensegrity-like structure by AM.

The large displacement static response of the double-T3 unit under uniaxial load was investigated from both the experimental and numerical points of view. The geometry of the unit was designed through parametric modelling and subsequently manufactured via SLA. Attention was focused on the design of the bases to be able to test the unit also under tensile forces. Experimental tests showed a bistable response of the designed unit, with high repeatability of results. The bistable mechanism of the unit was characterised by large relative rototranslations between the bases, as anticipated in the design phase. Such kinematics is permitted by the large deformations of the terminal links, which serve as compliant hinges. In principle, other boundary conditions could be considered as long as they activate the aforementioned bistable mechanism (e.g., a relative rotation between the bases could be applied).

When comparing the present results to previous studies (e.g., see [38,42]), several elements of novelty are ascertained. Under the fabrication standpoint, the compliant hinges introduced in the lattice reduce the magnitude of member shear forces, bending and twisting moments, keeping the force–displacement curve close enough to that of the corresponding pin-connected structure, thus preserving the bistable feature (cf. Fig. 3(c)). For a complex experimental characterisation of that response, samples were loaded both in compression and in tension during the displacement-control tests, following also the negative branch of the load–displacement curve. In particular, multiple tests performed on the same sample demonstrated the repeatability of the measurements with no significant alterations in the response or visible damage. Finally, the present results prove the possibility of additively manufacturing tensegrity-like lattices using a fairly accessible low-force stereolithography technology.

As to numerical simulations, it was verified that the stick-and-spring model provides a complete qualitative account of the response of the tensegrity-like unit. This model has the advantage of a reduced computational cost, and it is especially suitable for the simulation of assemblies composed of a large number of units. The implementation of beam elements or three-dimensional elements in finite-element numerical codes in order to obtain more accurate predictions will be the subject of future work. Follow-up studies can exploit the tensegrity characteristics, avoiding the need of pin joints or pretension cables, and investigate one-, two-, or three-dimensional tessellations assembled from tensegrity-like units obtained with the proposed procedure.

CRediT authorship contribution statement

Claudio Intrigila: Conceptualization, Methodology, Formal analysis, Investigation, Writing – original draft, Visualization. **Andrea Micheletti:** Conceptualization, Methodology, Formal analysis, Writing – original draft, Visualization. **Nicola A. Nodargi:** Conceptualization, Methodology, Writing – review & editing. **Edoardo Artioli:** Conceptualization, Methodology, Writing – review & editing. **Paolo Bisegna:** Conceptualization, Methodology, Writing – review & editing, Funding acquisition.

Declaration of competing interest

The authors declare that they have no known competing financial interests or personal relationships that could have appeared to influence the work reported in this paper.

Acknowledgements

The presented work was supported by the Italian Minister of University and Research through the project, "A bridge to the future: computational methods, innovative applications, experimental validations of new materials and technologies" (No. 2017L7X3CS) within the PRIN 2017 program.

Appendix A. Supplementary data

Supplementary material related to this article can be found online at https://doi.org/10.1016/j.addma.2022.102946.

References

[1] S. Walia, C.M. Shah, P. Gutruf, H. Nili, D.R. Chowdhury, W. Withayachumnankul, M. Bhaskaran, S. Sriram, Flexible metasurfaces and metamaterials: A review of materials and fabrication processes at micro-and nano-scales, Appl. Phys. Rev. 2 (1) (2015) 011303, http://dx.doi.org/10.1063/1.4913751.

[2] C. Bonatti, D. Mohr, Large deformation response of additively-manufactured FCC metamaterials: From octet truss lattices towards continuous shell mesostructures, Int. J. Plast. 92 (2017) 122–147, http://dx.doi.org/10.1016/j.ijplas.2017.02.003.

[3] M. Askari, D.A. Hutchins, P.J. Thomas, L. Astolfi, R.L. Watson, M. Abdi, M. Ricci, S. Laureti, L. Nie, S. Freear, R. Wildman, C. Tuck, M. Clarke, E. Woods, A.T. Clare, Additive manufacturing of metamaterials: A review, Addit. Manuf. 36 (2020) 101562, http://dx.doi.org/10.1016/j.addma.2020.101562.

[4] N.A. Fleck, V.S. Deshpande, M.F. Ashby, Micro-architectured materials: Past, present and future, Proc. Math. Phys. Eng. Sci. 466 (2121) (2010) 2495–2516, http://dx.doi.org/10.1098/rspa.2010.0215.

[5] T. Bückmann, N. Stenger, M. Kadic, J. Kaschke, A. Frölich, T. Kennerknecht, C. Eberl, M. Thiel, M. Wegener, Tailored 3D mechanical metamaterials made by dip-in direct-laser-writing optical lithography, Adv. Mater. 24 (20) (2012) 2710–2714, http://dx.doi.org/10.1002/adma.201200584.

[6] M.C. Messner, Optimal lattice-structured materials, J. Mech. Phys. Solids 96 (2016) 162–183, http://dx.doi.org/10.1016/j.jmps.2016.07.010.

[7] J.B. Berger, H.N.G. Wadley, R.M. McMeeking, Mechanical metamaterials at the theoretical limit of isotropic elastic stiffness, Nature 543 (7646) (2017) 533–537, http://dx.doi.org/10.1038/nature21075.

[8] L.R. Meza, G.P. Phlipot, C.M. Portela, A. Maggi, L.C. Montemayor, A. Comella, D.M. Kochmann, J.R. Greer, Reexamining the mechanical property space of three-dimensional lattice architectures, Acta Mater. 140 (2017) 424–432, http://dx.doi.org/10.1016/j.actamat.2017.08.052.

[9] M.H. Yousuf, W. Abuzaid, M. Alkhader, 4D Printed auxetic structures with tunable mechanical properties, Addit. Manuf. 35 (2020) 101364, http://dx.doi.org/10.1016/j.addma.2020.101364.

[10] C. Intrigila, N.A. Nodargi, P. Bisegna, The compressive response of additively-manufactured hollow truss lattices:An experimental investigation, Int. J. Adv. Manuf. Technol. 120 (2022) 3529–3541, http://dx.doi.org/10.1007/s00170-022-08716-0.

[11] T.A. Schaedler, A.J. Jacobsen, A. Torrents, A.E. Sorensen, J. Lian, J.R. Greer, L. Valdevit, W.B. Carter, Ultralight metallic microlattices, Science 334 (6058) (2011) 962–965, http://dx.doi.org/10.1126/science.1252291.

[12] L.R. Meza, S. Das, J.R. Greer, Strong, lightweight, and recoverable three-dimensional ceramic nanolattices, Science 345 (6202) (2014) 1322–1326, http://dx.doi.org/10.1126/science.1255908.

[13] X. Zheng, H. Lee, T.H. Weisgraber, M. Shusteff, J. DeOtte, E.B. Duoss, J.D. Kuntz, M.M. Biener, Q. Ge, J.A. Jackson, S.O. Kucheyev, N.X. Fang, C.M. Spadaccini, Ultralight, ultrastiff mechanical metamaterials, Science 344 (6190) (2014) 1373–1377, http://dx.doi.org/10.1126/science.1252291.

[14] S.C. Han, J.W. Lee, K. Kang, A new type of low density material: Shellular, Adv. Mater. 27 (37) (2015) 5506–5511, http://dx.doi.org/10.1002/adma.201501546.

[15] M. Maldovan, Sound and heat revolutions in phononics, Nature 503 (2013) 209–217, http://dx.doi.org/10.1038/nature12608.

[16] T. Brunet, J. Leng, O. Mondain-Monval, Soft acoustic metamaterials, Science 342 (2013) 323–324, http://dx.doi.org/10.1126/science.1241727.

[17] X.N. Liu, G.K. Hu, G.L. Huang, C.T. Sun, An elastic metamaterial with simultaneously negative mass density and bulk modulus, Appl. Phys. Lett. 98 (25) (2011) 251907, http://dx.doi.org/10.1063/1.3597651.

[18] N. Fang, D. Xi, J. Xu, M. Ambati, W. Srituravanich, C. Sun, X. Zhang, Ultrasonic metamaterials with negative modulus, Nature Mater. 5 (6) (2006) 452–456, http://dx.doi.org/10.1038/nmat1644.

[19] T.A.M. Hewage, K.L. Alderson, A. Alderson, F. Scarpa, Double-negative mechanical metamaterials displaying simultaneous negative stiffness and negative Poisson's ratio properties, Adv. Mater. 28 (46) (2016) 10323–10332, http://dx.doi.org/10.1002/adma.201603959.

[20] K. Wang, Y.H. Chang, Y. Chen, C. Zhang, B. Wang, Designable dual-material auxetic metamaterials using three-dimensional printing, Mater. Des. 67 (2015) 159–164, http://dx.doi.org/10.1016/j.matdes.2014.11.033.

[21] H. Cui, R. Hensleigh, D. Yao, D. Maurya, P. Kumar, M.G. Kang, S. Priya, X.R. Zheng, Three-dimensional printing of piezoelectric materials with designed anisotropy and directional response, Nature Mater. 18 (2019) 234–241, http://dx.doi.org/10.1038/s41563-018-0268-1.

[22] N.A. Nodargi, P. Bisegna, The saint-venant problem for general anisotropic piezoelectric cylinders with applications to smart metamaterials design, Appl. Math. Model. 93 (2021) 831–851, http://dx.doi.org/10.1016/j.apm.2021.01.003.

[23] F. Fraternali, L. Senatore, C. Daraio, Solitary waves on tensegrity lattices, J. Mech. Phys. Solids 60 (6) (2012) 1137–1144, http://dx.doi.org/10.1016/j.jmps.2012.02.007.

[24] C. Davini, A. Micheletti, P. Podio-Guidugli, On the impulsive dynamics of T3 tensegrity chains, Meccanica 51 (11) (2016) 2763–2776, http://dx.doi.org/10.1007/s11012-016-0495-y.

[25] A. Amendola, A. Krushynska, C. Daraio, N.M. Pugno, F. Fraternali, Tuning frequency band gaps of tensegrity mass–spring chains with local and global prestress, Int. J. Solids Struct. 155 (2018) 47–56, http://dx.doi.org/10.1016/j.ijsolstr.2018.07.002.

[26] D. De Tommasi, G. Puglisi, F. Trentadue, Elastic response of an optimal tensegrity-type metamaterial, Front. Mater. 6 (2019) 24, http://dx.doi.org/10.3389/fmats.2019.00024.

[27] I.J. Oppenheim, W.O. Williams, Geometric effects in an elastic tensegrity structure, J. Elasticity 59 (1) (2000) 51–65, http://dx.doi.org/10.1023/A:1011092811824.

[28] I.J. Oppenheim, W.O. Williams, Vibration of an elastic tensegrity structure, Eur. J. Mech. A Solids 20 (6) (2001) 1023–1031, http://dx.doi.org/10.1016/S0997-7538(01)01181-0.

[29] F. Fraternali, G. Carpentieri, A. Amendola, On the mechanical modeling of the extreme softening/stiffening response of axially loaded tensegrity prisms, J. Mech. Phys. Solids 74 (2015) 136–157, http://dx.doi.org/10.1016/j.jmps.2014.10.010.

[30] A. Amendola, G. Carpentieri, M. De Oliveira, R.E. Skelton, F. Fraternali, Experimental investigation of the softening–stiffening response of tensegrity prisms under compressive loading, Compos. Struct. 117 (2014) 234–243, http://dx.doi.org/10.1016/j.compstruct.2014.06.022.

[31] A. Micheletti, Bistable regimes in an elastic tensegrity system, Proc. R. Soc. A. 469 (20130052) (2013) 20130052, http://dx.doi.org/10.1098/rspa.2013.0052.

[32] F. Fraternali, G. Carpentieri, A. Amendola, R.E. Skelton, V.F. Nesterenko, Multiscale tunability of solitary wave dynamics in tensegrity metamaterials, Appl. Phys. Lett. 105 (20) (2014) 201903, http://dx.doi.org/10.1063/1.4902071.

[33] A. Micheletti, G. Ruscica, F. Fraternali, On the compact wave dynamics of tensegrity beams in multiple dimensions, Nonlinear Dynam. 98 (4) (2019) 2737–2753, http://dx.doi.org/10.1007/s11071-019-04986-8.

[34] J. Rieffel, F. Valero-Cuevas, H. Lipson, Automated discovery and optimization of large irregular tensegrity structures, Comput. Struct. 87 (5) (2009) 368–379, http://dx.doi.org/10.1016/j.compstruc.2008.11.010.

[35] K. Liu, J. Wu, G.H. Paulino, H.J. Qi, Programmable deployment of tensegrity structures by stimulus-responsive polymers, Sci. Rep. 7 (2015) 3511, http://dx.doi.org/10.1038/s41598-017-03412-6.

[36] A. Amendola, E. Hernández-Nava, R. Goodall, I. Todd, R.E. Skelton, F. Fraternali, On the additive manufacturing, post-tensioning and testing of bi-material tensegrity structures, Compos. Struct. 131 (2015) 66–71, http://dx.doi.org/10.1016/j.compstruct.2015.04.038.

[37] H. Lee, Y. Jang, J.K. Choe, S. Lee, H. Song, J.P. Lee, N. Lone, J. Kim, 3D-Printed programmable tensegrity for soft robotics, Sci. Robot. 5 (45) (2020) eaay9024, http://dx.doi.org/10.1126/scirobotics.aay9024.

[38] Z. Vangelatos, A. Micheletti, C.P. Grigoropoulos, F. Fraternali, Design and testing of bistable lattices with tensegrity architecture and nanoscale features fabricated by multiphoton lithography, Nanomaterials 10 (4) (2020) 652, http://dx.doi.org/10.3390/nano10040652.

[39] K. Pajunen, P. Johanns, R.K. Pal, J.J. Rimoli, C. Daraio, Design and impact response of 3D-printable tensegrity-inspired structures, Mater. Des. 182 (2019) 107966, http://dx.doi.org/10.1016/j.matdes.2019.107966.

[40] K. Pajunen, P. Celli, C. Daraio, Prestrain-induced bandgap tuning in 3D-printed tensegrity-inspired lattice structures, Extreme Mech. Lett. 44 (2021) 101236, http://dx.doi.org/10.1016/j.eml.2021.101236.

[41] J. Bauer, J.A. Kraus, C. Crook, J.J. Rimoli, L. Valdevit, Tensegrity metamaterials: Toward failure-resistant engineering systems through delocalized deformation, Adv. Mater. 33 (10) (2021) 2005647, http://dx.doi.org/10.1002/adma.202005647.

[42] A. Micheletti, C. Intrigila, N.A. Nodargi, E. Artioli, F. Fraternali, P. Bisegna, Modeling and design of periodic lattices with tensegrity architecture and highly nonlinear response, in: M. Fragiadakis M. Papadrakakis (Ed.), COMPDYN 2021: 8th ECCOMAS Thematic Conference on Computational Methods in Structural Dynamics and Earthquake Engineering, 2021, pp. 1848–1855, http://dx.doi.org/10.7712/120121.8605.19232.

[43] H. Yang, L. Ma, 1D To 3D multi-stable architected materials with zero Poisson's ratio and controllable thermal expansion, Mater. Des. 188 (2020) 108430, http://dx.doi.org/10.1016/j.matdes.2019.108430.

[44] H. Yasuda, T. Tachi, M. Lee, J. Yang, Origami-based tunable truss structures for non-volatile mechanical memory operation, Nature Commun. 8 (1) (2017) 1–7, http://dx.doi.org/10.1038/s41467-017-00670-w.

[45] S. Shan, S.H. Kang, J.R. Raney, P. Wang, L. Fang, F. Candido, J.A. Lewis, K. Bertoldi, Multistable architected materials for trapping elastic strain energy, Adv. Mater. 27 (29) (2015) 4296–4301, http://dx.doi.org/10.1002/adma.201501708.

[46] F. Pan, Y. Li, Z. Li, J. Yang, B. Liu, Y. Chen, 3D Pixel mechanical metamaterials, Adv. Mater. 31 (25) (2019) 1900548, http://dx.doi.org/10.1002/adma.201900548.

[47] Y. Chen, L. Jin, Reusable energy-absorbing architected materials harnessing snapping-back buckling of wide hyperelastic columns, Adv. Funct. Mater. (2021) 2102113, http://dx.doi.org/10.1002/adfm.202102113.

[48] J. Meaud, K. Che, Tuning elastic wave propagation in multistable architected materials, Int. J. Solids Struct. 122 (2017) 69–80, http://dx.doi.org/10.1016/j.ijsolstr.2017.05.042.

[49] L.L. Howell, Compliant mechanisms, in: J. McCarthy (Ed.), 21st Century Kinematics, Springer, 2013, pp. 189–216, http://dx.doi.org/10.1007/978-1-4471-4510-3_7.

[50] A. Favata, A. Micheletti, P. Podio-Guidugli, A nonlinear theory of prestressed elastic stick-and-spring structures, Internat. J. Engrg. Sci. 80 (2014) 4–20, http://dx.doi.org/10.1016/j.ijengsci.2014.02.018.

[51] A. Amendola, A. Favata, A. Micheletti, On the mechanical modeling of tensegrity columns subject to impact loading, Front. Mater. 5 (2018) 22, http://dx.doi.org/10.3389/fmats.2018.00022.

[52] L.Y. Zhang, Y. Li, Y.P. Cao, X.Q. Feng, H. Gao, Self-equilibrium and superstability of truncated regular polyhedral tensegrity structures: A unified analytical solution, Proc. R. Soc. A. 468 (2147) (2012) 3323–3347, http://dx.doi.org/10.1098/rspa.2012.0260.

[53] J.J. Rimoli, R.K. Pal, Mechanical response of 3-dimensional tensegrity lattices, Compos. B. Eng. 115 (2017) 30–42, http://dx.doi.org/10.1016/j.compositesb.2016.10.046.

[54] A.G. Tibert, S. Pellegrino, Review of form-finding methods for tensegrity structures, Int. J. Space Struct. 18 (4) (2003) 209–223, http://dx.doi.org/10.1260/026635103322987940.

[55] R. Motro, Tensegrity: Structural Systems for the Future, Kogan Page Science, London, U.K, 2003.

[56] R.E. Skelton, M.C. de Oliveira, Tensegrity Systems, Springer, Boston, MA, US, 2009, http://dx.doi.org/10.1007/978-0-387-74242-7.

[57] Y. Li, X.Q. Feng, Y.P. Cao, H. Gao, A Monte Carlo form-finding method for large scale regular and irregular tensegrity structures, Int. J. Solids Struct. 47 (14) (2010) 1888–1898, http://dx.doi.org/10.1016/j.ijsolstr.2010.03.026.

[58] F. Maceri, M. Marino, G. Vairo, An operative algebraic formulation for the unilaterally-constrained mechanical problem of smart tensegrities, Int. J. Solids Struct. 51 (19–20) (2014) 3333–3349, http://dx.doi.org/10.1016/j.ijsolstr.2014.05.021.

[59] N. Pietroni, A. Vaxman, D. Panozzo, P. Cignoni, Position-based tensegrity design, ACM Trans. Graph. 36 (2017) 1–14, http://dx.doi.org/10.1145/3130800.3130809.

[60] K. Liu, T. Zegard, P.P. Pratapa, G.H. Paulino, Unraveling tensegrity tessellations for metamaterials with tunable stiffness and bandgaps, J. Mech. Phys. 131 (2019) 147–166, http://dx.doi.org/10.1016/j.jmps.2019.05.006.

[61] A. Al Sabouni-Zawadzka, W. Gilewski, Smart metamaterial based on the simplex tensegrity pattern, Materials 11 (5) (2018) http://dx.doi.org/10.3390/ma11050673.

[62] C.R. Calladine, S. Pellegrino, First-order infinitesimal mechanisms, Int. J. Solids Struct. 27 (4) (1991) 505–515, http://dx.doi.org/10.1016/0020-7683(91)90137-5.

[63] C.R. Calladine, Buckminster Fuller's 'tensegrity' structures and Clerk Maxwell's rules for the construction of stiff frames, Int. J. Solids Struct. 14 (2) (1978) 161–172, http://dx.doi.org/10.1016/0020-7683(78)90052-5.

[64] L.C. Montemayor, L.R. Meza, J.R. Greer, Design and fabrication of hollow rigid nanolattices via two-photon lithography, Adv. Eng. Mater. 16 (2) (2014) 184–189, http://dx.doi.org/10.1002/adem.201300254.

[65] R. Tu, H.A. Sodano, Additive manufacturing of high-performance vinyl ester resin via direct ink writing with uv-thermal dual curing, Addit. Manuf. 46 (2021) 102180, http://dx.doi.org/10.1016/j.addma.2021.102180.

[66] C. Riccio, M. Civera, O. Grimaldo Ruiz, P. Pedullà, M. Rodriguez Reinoso, G. Tommasi, M. Vollaro, V. Burgio, C. Surace, Effects of curing on photosensitive resins in sla additive manufacturing, Appl. Mech. 2 (4) (2021) 942–955, http://dx.doi.org/10.3390/applmech2040055.

[67] Standard Test Method for Tensile Properties of Plastics, ASTM D638-14, 2014, http://dx.doi.org/10.1520/D0638-14, ASTM International, West Conshohocken, PA.